

Effect of electrode configuration on the sensitivity of nucleic acid detection in a non-planar, flow-through, porous interdigitated electrode

Cite as: Biomicrofluidics 13, 064118 (2019); doi: 10.1063/1.5126452

Submitted: 3 September 2019 · Accepted: 6 November 2019 ·

Published Online: 21 November 2019



View Online



Export Citation



CrossMark

Yu-Hsuan Cheng,¹ Pedro Antonio Reis Moura,¹ Li Zhenglong,¹ Lixin Feng,² Siril Arokiam,¹ Juliana Yang,² Mahima Hariharan,¹ and Sagnik Basuray^{1,2,a)}

AFFILIATIONS

¹Department of Chemical and Materials Engineering, New Jersey Institute of Technology, Newark, New Jersey 07102, USA

²Department of Biomedical Engineering, New Jersey Institute of Technology, Newark, New Jersey 07102, USA

Note: This article is part of the special topic, *Festschrift for Professor Hsueh-Chia Chang*.

a) Author to whom correspondence should be addressed: sbasuray@njit.edu

ABSTRACT

Electrical impedance spectroscopy (EIS) sensors, though rapid and cost-effective, often suffer from poor sensitivity. EIS sensors modified with carbon-based transducers show a higher conductance, thereby increasing the sensitivity of the sensor toward biomolecules such as DNA. However, the EIS spectra are compromised by the parasitic capacitance of the electric double layer (EDL). Here, a new shear-enhanced, flow-through nonporous, nonplanar interdigitated microelectrode sensor has been fabricated that shifts the EDL capacitor to high frequencies. Enhanced convective transport in this sensor disrupts the diffusion dynamics of the EDL, shifting its EIS spectra to high frequency. Concomitantly, the DNA detection signal shifts to high frequency, making the sensor very sensitive and rapid with a high signal to noise ratio. The device consists of a microfluidic channel sandwiched between two sets of top and bottom interdigitated microelectrodes. One of the sets of microelectrodes is packed with carbon-based transducer material such as carboxylated single-walled carbon nanotube (SWCNT). Multiple parametric studies of three different electrode configurations of the sensor along with different carbon-based transducer materials are undertaken to understand the fundamental physics and electrochemistry. Sensors packed with SWCNT show femtomolar detection sensitivity from all the different electrode configurations for a short target-DNA. A 20-fold jump in the signal is noticed from the unique working electrode configuration in contrast to the other electrode configurations. This demonstrates the potential of the sensor to have a significant increase in detection sensitivity for DNA and other biomolecules.

Published under license by AIP Publishing. <https://doi.org/10.1063/1.5126452>

INTRODUCTION

Deoxyribonucleic acid/ribonucleic acid (DNA/RNA) are fundamental biomarkers for the identification of specific diseases.^{1–3} For example, in a liquid biopsy, detecting and long-term tracking of circulating tumor DNA (ctDNA) in human blood are critical for early-stage cancer detection, treatment, and during remission.⁴ Analysis of ctDNA is challenging due to its extremely low concentration in human blood (<1% in many cases).⁵ Hence, sensitive detection of ctDNA is one of the significant issues in this field. PCR-based amplification technologies are well developed with sensitivities of less than 50 ng.^{6–9} However, most PCR-based methods need complex, expensive, and precise chemical procedures to

acquire a reliable result. Besides, PCR amplification technologies pass through a series of reactions to increase the ctDNA concentration. Hence, the final reading often does not reflect the actual ctDNA concentration in the human body. Hybridization of target ctDNA molecule to short single-stranded DNA (ssDNA), called oligonucleotide, is the preferred method of detection of ctDNA.¹⁰

Electrochemical biosensors use faradaic techniques like cyclic voltammetry¹¹ and pulse voltammetry¹² or nonfaradaic techniques like electrical impedance spectroscopy (EIS).¹³ Electrochemical biosensors provide automatic tracking and detection, a user-friendly platform, and are of low cost.¹⁰ Generally, the design of a biosensor consists of an analyte (with the target molecule), a bioreceptor (the capture molecule), a transducer, electronic components, and a

display.¹⁴ The ssDNA oligonucleotide used for the detection of ctDNA has a 5' modification designed to bind to the transducer. Electrochemical sensors convert the hybridization signal (binding of a ctDNA to an oligo) to an equivalent electrical/electrochemical signal. Currently, the detection sensitivity of electrochemical sensors for ctDNA is around 10 pM without expensive electrode modifications or extensive protocols.¹⁵ Hence, there is a demand for simple electrochemical sensors capable of detecting low amounts of ctDNA.

Among electrochemical biosensors, EIS-based biosensors have been used for detecting different biomarkers, such as proteins,¹⁶ antibodies,¹⁷ or DNA.^{1,12,13} EIS-based sensors detect changes in the electric current from the electrode surface on the application of a sinusoidal AC voltage. The changes are caused by the immobilization of the target analyte (DNA, antigen, among others) to receptors/molecule receptors on the electrode surface. Device sensitivity determines whether one can detect the physical or chemical changes on the electrode surface due to target binding. This electrochemical signal increases with the use of a nanomaterial as a transducer as has been shown elsewhere.^{18–20} Carbon nanotubes (CNTs) are one of many common materials used as a transducer in electrochemical biosensors.²¹ Due to its high electrical conductivity and high surface area to volume ratios, CNTs make an extraordinary transducer material. The surface of the CNT can also be easily modified and bonded to ssDNA oligonucleotides by standard coupling and functionalization reactions.^{22,23}

The problem with EIS-based sensors is the electrical double layer (EDL). EDL is a parasitic capacitor that reduces the sensor's sensitivity and increases the noise. Our group has introduced a novel electrochemical platform that uses shear-enhanced, flow-through, nanoporous, nonplanar interdigitated microelectrode (NP-μIDE) that allows for a significant reduction of the noise from the EDL. Unlike in planar interdigitated microelectrode, where the electric field is only at the vicinity of the electrode surface, in NP-μIDE the electric field penetrates throughout the channel. This allows any target molecules captured anywhere in the channel to perturb (sensor signal) the electric field between the electrodes, significantly enhancing the sensitivity of NP-μIDE. Further, microelectrode (μEs) as electrochemical transducers offer the advantage of high collection efficiencies, a low response time that favors rapid detection, low ohmic drop, easy fabrication over multiple substrates, readiness for miniaturization, and eliminates the need for a reference electrode allowing easy integration with microfluidic chips for multiplexed analytical platforms.²⁴

In this work, we show the DNA sensitivity of NP-μIDE that packs carbon-based transducer materials between the bottom and top microelectrodes. As has been shown earlier and here, our fabrication and device integration process is simple, easy to set up, cost-effective, and requires minimal operator handling/expertise.²⁵ NP-μIDE with packed carbon materials increases convective transport, disrupting the diffusive dynamics that govern the EDL. Hence, the EDL capacitor signal moves to higher frequencies.^{25,26} These allow the measurement of the EIS sensor signal at significantly higher frequencies reducing the noise and making the system rapid. Different types of carbon transducer materials such as single-wall carbon nanotube (SWCNT), aligned multiwall carbon nanotube (aligned-MWCNT), single-wall carbon nanotube with carboxyl groups (SWCNT-COOH), and carbon nanofiber (CNF) are tested in multiple electrode configurations with different

voltages and potassium chloride (KCl) concentrations. ssDNA oligo probes are functionalized to the carboxylate CNT using standard EDC-NHS coupling. The device is tested with short target-DNA. The detection limit is femtomolar. Further, the EIS sensor showed that among different electrode configurations, DNA detection sensitivity is higher for specific electrode configurations. To summarize, the increased sensitivity of NP-μIDE over other CNT based microelectrode sensors is due to (1) high SNR due to the use of microelectrodes, (2) enhanced electric field penetration from the nonplanar microelectrodes, and (3) the porous transducer layer that shifts the EDL to higher frequencies resulting in even more increase in SNR.

METHODS AND MATERIALS

Reagents and instruments

Standard glass slides (1304G) with ground edges, 90° corners, and size $25 \times 75 \times 1 \text{ mm}^3$ are ordered from Globe Scientific Inc. (USA). The de-ionized (DI) water used in the experiments is obtained from a Milli Q Direct 8 Water Purification System with a conductivity of $7.9 \mu\text{S}/\text{cm}$. A double-sided polypropylene (PP) tape (90880) with SR-26 silicone pressure-sensitive adhesives on both sides is obtained from ARcare, USA. The thickness of the tape is 142 μm including the PP layer and the two adhesives. Potassium chloride (KCl), ACS grade, is acquired from British Drug Houses (BDH). The 4294A Precision Impedance Analyzer from Keysight Technologies is used for all the EIS measurements. Different transducer materials such as carbon nanofiber (CNF, 95%+), short single-wall carbon nanotube (SWCNT, 98%+), carboxylic acid functionalized short single-walled carbon nanotube (C-SWCNT, 98%+), and aligned multiwall carbon nanotube (MWCNT, 95%+) are all acquired from US Research Nanomaterials Inc. Fabrication of the top and bottom microelectrode glass slide is carried out in the Nano-fabrication facility at CUNY Advanced Science Research Center.

Device fabrication

Cleaning steps for the standard glass slides involve (1) two 10 min 1:3 Piranha washes for removal of organic contaminants and (2) an AMD wash protocol for removal of any residual contaminants from the Piranha Wash. The AMD wash involves consecutively rinsing the glass slide by acetone, isopropanol, methanol, and DI water. Following the AMD wash, the glass slide is dried using a Nitrogen gun. (3) The glass slide is heated to 130 °C for 30 min to eliminate any surface-bound moisture. Hexamethyldisilazane (HMDS) is spun onto the glass slides in two spins of 400 rpm for 15 s and 1000 rpm for 45 s with a ramping rate of 200 rpm/s using a Brewer Science Cee's spin coater to promote photoresist adhesion. A positive tone photoresist AZ 1512 is spun onto the glass slide using two spins of 500 rpm for 10 s and 3000 rpm for 45 s at a ramping rate of 200 rpm/s and then soft-baked at 110 °C for 60 s for a conformal coat of 1.39 μm. For contact lithography, an EV Group's EVG620 mask aligner is used to expose the glass slides with photoresist to an electrode mask. The UV exposure dosage is 350 J/m². Post exposure, the slides are developed in the fresh AZ 300 MIF Developer for 35 s, followed by a de-ionized water wash and nitrogen

drying. The pattern is checked for accuracy under a microscope. An AJA Orion 8E Evaporator System for electron beam (e-beam) is used to deposit 10 nm of titanium followed by 100 nm of gold (both at 2 Å/s) on the patterned glass slides. The electrode geometry is developed post-deposition using lift-off by immersing in acetone bath after one day. The microchannel is constructed out of ARcare® 90880 polypropylene double-sided tape. The microfluidic channel is cut to dimension using the Cricut®. The dimensions of the channel are 48 mm (L) × 500 μm (W) × 142 μm (H). The final device consists of a microchannel made from the double-sided tape sandwiched between a top and bottom patterned microelectrode. Inlet and outlet holes for fluid flow are drilled by a 1 mm diamond drill bit onto the top microelectrode glass slide. The adhesive on each side of the tape is attached to the bottom and the top microelectrode glass slide to form the NP-μIDE.

Transducer packing and device integration

The packing of the channel with transducer material is done using the following protocol. The liner from the bottom side of the double-sided tape is removed to expose the silicon adhesive. The channel is cut into the double-sided tape using the Cricut machine.

The cut tape is first aligned to the bottom microelectrode glass slide. Post alignment, the double-sided tape is fixed to the bottom microelectrode glass slide using the exposed silicon adhesive. The transducer material is mixed with 1× PBS to form a slurry. The slurry is loaded into the channel to create a tight packing with the top liner still on. The top liner is then removed to expose the silicon adhesive. The top microelectrode slide is aligned to the channel containing the transducer material (CNF, SWCNT, C-SWCNT, or MWCNT). The alignment is carried out under a microscope to ensure the interdigititation of the nonplanar electrodes.

KCl run protocol

The device is packed with CNF, SWCNT, C-SWCNT, or MWCNT using the transducer packing protocol as described before. The KCl is diluted with DI water to get the required KCl concentrations from 1M to 1 μM. These devices are connected to the Impedance analyzer, Agilent 4294A, for EIS readings using standard electrical connections (Fig. 1). The devices are first washed with DI water for 1 h. After the wash procedure, KCl flows through the device at 1 μl/min. The EIS signal for a KCl concentration is taken after 1 h.

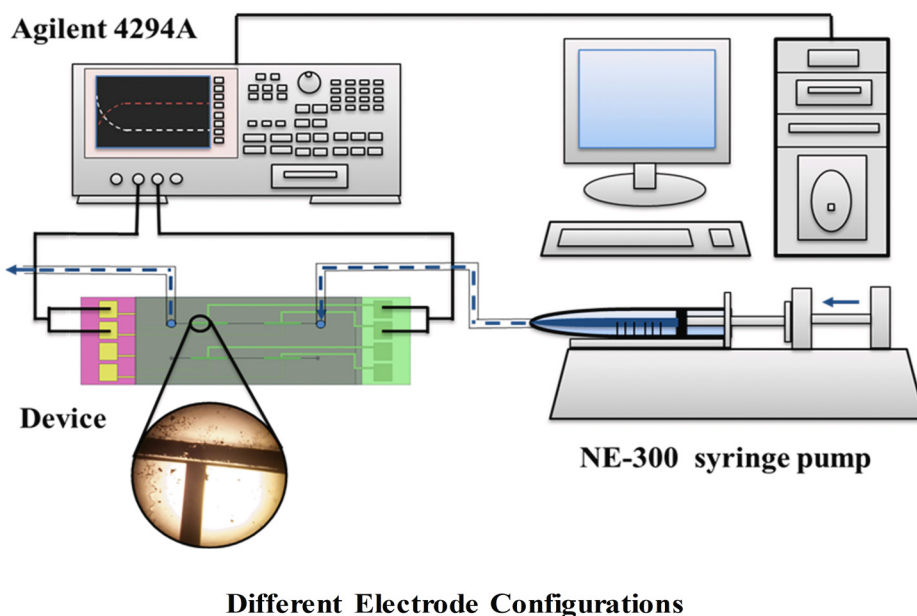
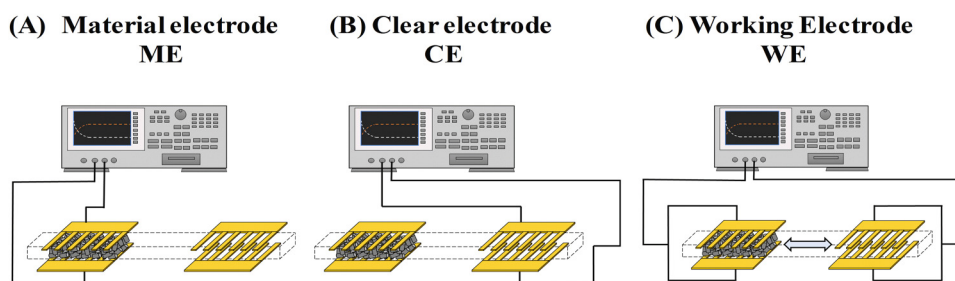


FIG. 1. Diagram of the experiential setup. The microfluidic devices are connected to an EIS machine (Agilent 4294A) from the NP-μIDE device. The solvent is controlled using a NE-300 syringe pump with a flow rate of 1 μl/min. (a) Material electrode (ME) configuration. (b) Clear electrode (CE) configuration. (c) Working electrode (WE) configuration.



CNT functionalization of SWCNT

Probe-DNA and target-DNA oligo with the sequence of 5'-/-5AmMC6/CGTCCAAGCGGGCTGACTCATCAAG-3' and 5'-CTT GATGAGTCAGCCGCTTGGACG-3', respectively, are acquired from Integrated DNA Technologies (IDT). A10807 1-(3-dimethylaminopropyl)-3-ethyl carbodiimide hydrochloride (EDAC) and A10312 *N*-Hydroxysuccinimide (NHS) are purchased from Alfa Aesar with 98%+ purity. 2-(*N*-Morpholino) ethanesulfonic acid hydrate (MES) is acquired from Sigma-Aldrich with 99.5%+ purity. Phosphate Buffered Saline (PBS) tablets are purchased from VWR. 30 mg of the C-SWCNT is vortexed/washed in the 0.1M MES buffer and centrifuged in a 1.7 ml Eppendorf at 6000 RPM (GeneMate Minifuge) thrice. During the wash, the suspension is replaced with fresh MES. The supernatant is taken out and activated with the EDC-NHS coupling reaction with probe-DNA oligo in 1× PBS solvent overnight. The DNA-functionalized C-SWCNT is washed in 1× PBS (pH 7.4) and preserved in the refrigerator.

DNA run protocol

The DNA-functionalized C-SWCNT device is connected to the Impedance analyzer using standard electrical connections, as shown in Fig. 1. Target-DNA oligo concentrations are diluted to 1 μM, 1 nM, 10 pM, 1 pM, 0.1 pM, and 1 fM with 1× PBS (pH 7.4). The DNA oligo sensor protocol involves the following steps. A NE-300 syringe pump from New Era Pump Systems, Inc. (USA) is connected to the inlet of the device. The device is first washed with 1× (pH 7.4) PBS solution at a flow rate of 1 μl/min for 2 h or until the EIS signal from the device stabilizes. The stabilization of the EIS signal is interpreted as two EIS measurements that do not change when taken 5 min apart. This stabilized EIS signal taken in 1× PBS is treated as the baseline measurement. Post stabilization, the 1× PBS solution is switched to the 1M Ethanolamine (99%+ pure from Alfa Aesar) in 1× PBS for 90 min. Ethanolamine blocks nonreacted carboxy groups, which will reduce the nonspecific adsorption of the target-DNA in the device.^{27–29} Post blocking, the device is washed with 1× PBS for 2 h to remove any remaining ethanolamine. Target-DNA oligos flow into the system at 1 μl/min for 2 h. Post target-DNA oligo passage, the solution is switched back to

1× (pH 7.4) PBS solution (washing solution). The device is rinsed with 1× (pH 7.4) PBS solution at a flow rate of 1 μl/min for 3 h and 30 min to remove any unspecific bound target-DNA in the device. This difference between the EIS signal from the pre- and post-PBS wash is interpreted as the target-DNA oligo capture signal.

RESULTS AND DISCUSSIONS

Figure 1 shows the working of the sensor device. It is worthwhile to note that the sensor has a 2 × 2 configuration, i.e., two NP-μIDE sets are placed in a single channel. One of the NP-μIDE set is packed with transducer material. The other NP-μIDE is empty. Flow passes through both of these NP-μIDE sets, one after another. EIS data are recorded by different electrode configurations that are made using these two sets of NP-μIDE. A material electrode configuration (ME) is the EIS signal from the first set of NP-μIDE packed with transducer material [Fig. 1(a)]. The clear electrode (CE) configuration is the EIS signal from the second set of NP-μIDE that does not have any transducer material [Fig. 1(b)]. Finally, the working electrode (WE) configuration is a unique take on the electrodes. The first set of NP-μIDE with packing is shorted together to form a single electrode (working). The second set of NP-μIDE is also shorted to form a single electrode (counter). The EIS signal is now taken between the working and the counter electrodes [Fig. 1(c)]. WE configuration allows us to observe any changes that take place in the packed NP-μIDE set and contrast it against the empty NP-μIDE set of electrodes.

Each electrode configuration (ME, CE, and WE) is examined in detail to understand what electrochemical properties are measured by what electrode configuration. Figure 2(a) shows the Nyquist curve for the EIS signal from SWCNT ME in 0.01M KCl concentration at different voltages. It is worthwhile to note that the EIS signal shows a series of LR circuit. Further, the packed electrode behaves like a pure ohmic resistor at low frequency due to the high electronic conductivity of SWCNT. It is worthwhile to note that SWCNT acts as a pure conductor in the experimental voltage range as has been seen elsewhere.²⁷ Hence, capacitive behavior of the electrode is absent. At higher frequency, the Nyquist spectra

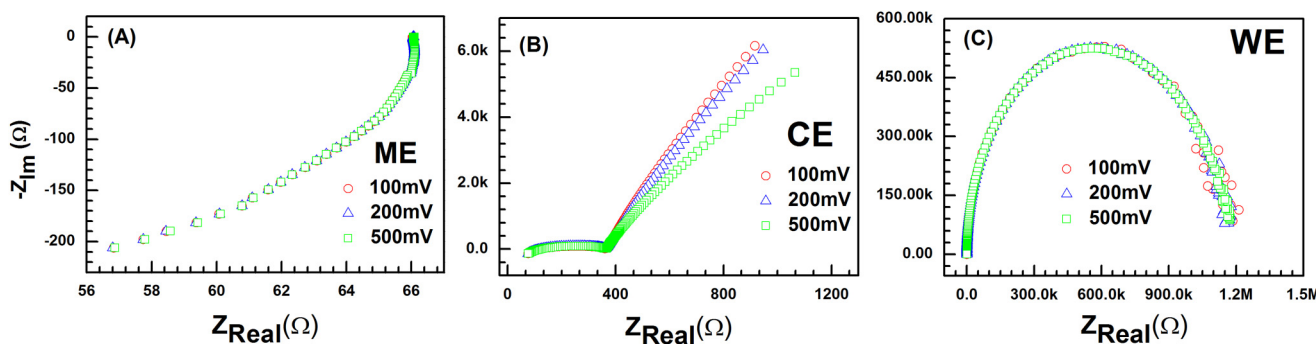


FIG. 2. EIS spectra of SWCNT packed NP-μIDE devices in 0.01M KCl for different configurations and voltages (a) ME configuration. (b) CE configuration. (c) WE configuration.

show up as an inductor. The packing of the conducting SWCNT in the channel is similar to that of twisted conducting wire. Like a twisted conducting wire in an applied electric field, the packed SWCNT behaves like an inductor at high frequency. It is interesting to note that the voltage does not have any effect on the Nyquist curve.

CE shows an atypical Randles circuit electrode semicircle in the Nyquist plot [Fig. 2(b)]. The electrode response between the NP- μ IDE shows a similar diffusion dominated behavior to the EIS response as seen from interdigitated gold planar electrodes.²⁸ The same diffusion layer is responsible for the Warburg impedance seen at the lower frequency. The NP- μ IDE geometry results in a finite diffusion layer. That results in a nonideal Warburg that is more capacitive, as has been seen elsewhere.²⁹ Further, as expected, with an increase in voltage, the diffusion layer increases, which results in a progressively less capacitive Warburg resistor.²⁹ The WE combination combines the above two configurations to result in a parallel RC circuit, as shown in Fig. 2(c). However, the RC of the EIS spectra from the WE shows a significantly high R. It is hypothesized that this large R is due to the significant distance between the two sets of NP- μ IDE (~10 mm). We speculate that at lower voltages and low frequency, the scatter in the system is due to increased drift current as has been seen elsewhere with high resistance.

A critical element for an EIS sensor is the response to electrolytes, specifically the conductivity of the electrolyte. Figure 3(a) shows that for SWCNT ME, the EIS spectra are still an LR circuit in series at low KCl concentrations while at higher concentrations, a small RC circuit starts to appear. This RC at the higher KCl concentrations can be attributed to the increased capacitance of the EDL. The charge relaxation frequency ($1/RC$) decreases substantially at higher values of C, which allows the RC to dominate at the lower frequencies (L, the inductor is weak at low frequency). It is important to note that there are two current paths that help us to understand the origin of the C at higher concentrations and low frequencies. The first current path is directly through the packed SWCNT that leads to a purely resistive EIS signal at low frequency. The second current path is the ionic current in the electrolyte surrounding the SWCNT and the electrodes. At low concentrations, the electronic conductivity of the electrolyte is significantly lower in

comparison to the packed SWCNT, and hence the current chiefly passes through the SWCNT. However, at higher concentrations, the ionic current is also significant. These ionic currents can lead to a charge accumulation near the electrodes/SWCNT. It is interesting to note that this is similar to the EIS signal observed from gold electrodes, albeit shifted by frequency due to the L present across most of the frequency range. From Fig. 4(a), the only material that does not show this RC behavior at low frequency is the aligned-MWCNT. It can be hypothesized to the much higher conductivity of the MWCNT (>1250 s/cm) in comparison to the other materials. Further, the SWCNT-COOH group shows the largest RC signature among all the different materials at high concentrations [Fig. 3(a)]. This is due to the presence of charged moieties (-COOH) on its surface that leads to an enhanced capacitor.³⁰ This dominates the LR circuit even more than the other materials at the high concentrations. Hence, SWCNT-COOH crosses the resistance axis at a lower value than the MWCNT even though it has a lower conductivity than the MWCNT (as can be seen at the lower concentrations).

The CE [Fig. 3(b)] follows a traditional Randles circuit with the charge transfer resistance (R_{ct}) decreasing with an increase in KCl concentration. The WE [Figs. 3(c) and 4(b)] also follows a similar Randles circuit though with a much higher R_{ct} than the CE. The increase in R_{ct} can be attributed to the distance between two sets of NP- μ IDE. For the WE, the EIS spectra are more scattered at the lower concentrations and the lower frequencies [Figs. 3(c) and 4(b)]. The problem of noise at the lower frequencies is due to the drift of the current at high R_{ct} and low frequency. Hence, this scatter is more pronounced in the lowest KCl concentrations, which has the highest R_{ct} in WE. In this manuscript, however, we are not too worried about the noise in the WE as for DNA detection experiments, the electrolyte will have a high ionic concentration. DNA is much more stable at high ionic concentrations.³¹ Our electrolyte is 1× PBS media with a conductivity of 13 500–17 000 μ S/cm, which is equivalent to 0.1M KCl (12 880 μ S/cm). Hence, EIS spectra taken in 1× PBS should not have any scatter at the low frequency.

In Fig. 4 (left panel, top row), the EIS response of SWCNT and the aligned-MWCNT is shown for 1M KCl concentration.

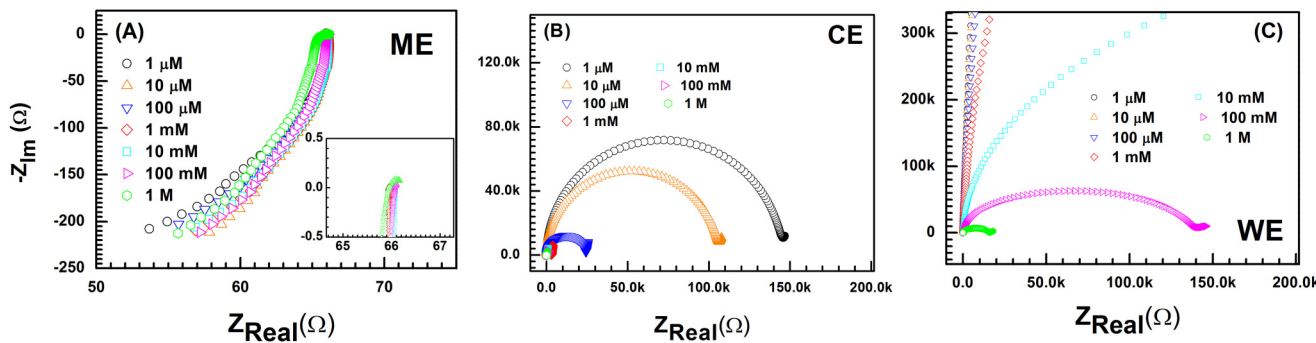


FIG. 3. The effect of KCl concentration on NP- μ IDE with single-wall carbon nanotube (SWCNT) is shown for (a) ME configuration, (b) CE configuration, and (c) WE configuration.

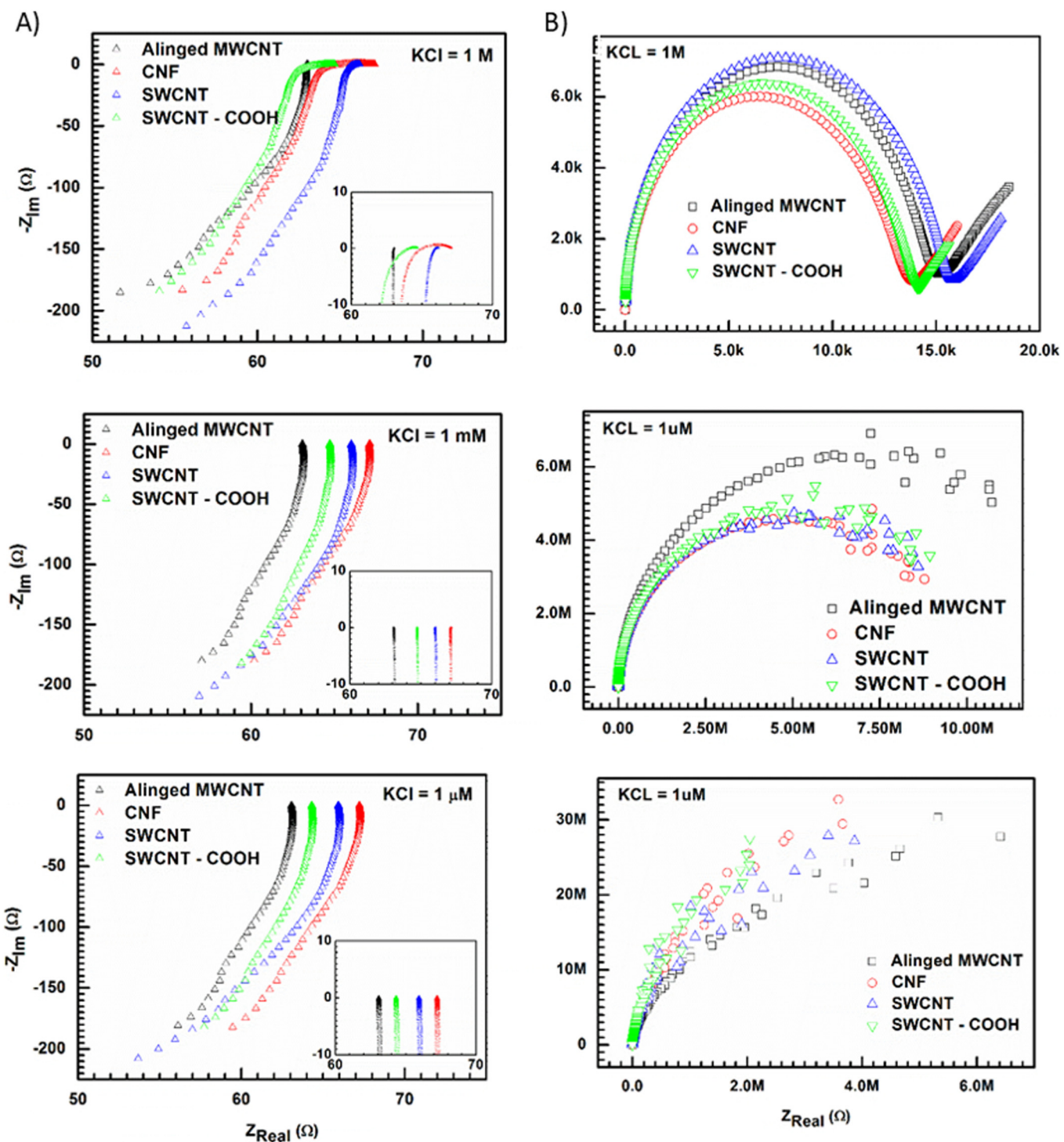


FIG. 4. The effect of KCl concentration on NP- μ IDE with different packing materials, namely, single-wall carbon nanotube (SWCNT), aligned multiwall carbon nanotube (AMWCNT), single-wall carbon nanotube with carboxyl groups (SWCNT-COOH), and carbon nanofiber (CNF) is shown for (a) ME configuration at 1M, 1mM, and 1 μ M KCl concentrations and (b) WE at 1M, 1mM, and 1 μ M KCl concentrations.

Atypical matrices used in a sensor to detect circulating tumor DNA will have high conductivities like 1M KCl.³¹ For a sensor approach, capture DNA will be coupled to the carboxylate groups on the surface of the SWCNT or the aligned-MWCNT. The target-DNA will bind to this capture DNA, which should change the ionic current to the SWCNT or the aligned-MWCNT. This change in the ionic current is a perturbation in the total current. The bulk of the total current is the electrode current that will flow thought the SWCNT or the aligned-MWCNT from the bottom μ E to the top μ E. However, as the aligned-MWCNT has a much lower resistance than the SWCNT [Fig. 4 (left panel, top row)], the contribution of the ionic current to the total current will be significantly less for aligned-MWCNT in comparison to SWCNT. Hence, SWCNT will have a higher sensitivity to any changes on its surface (ionic current) in comparison to the aligned-MWCNT. Between aligned-MWCNT and SWCNT, it can thus be concluded that indeed SWCNT is a better transducer packing material than

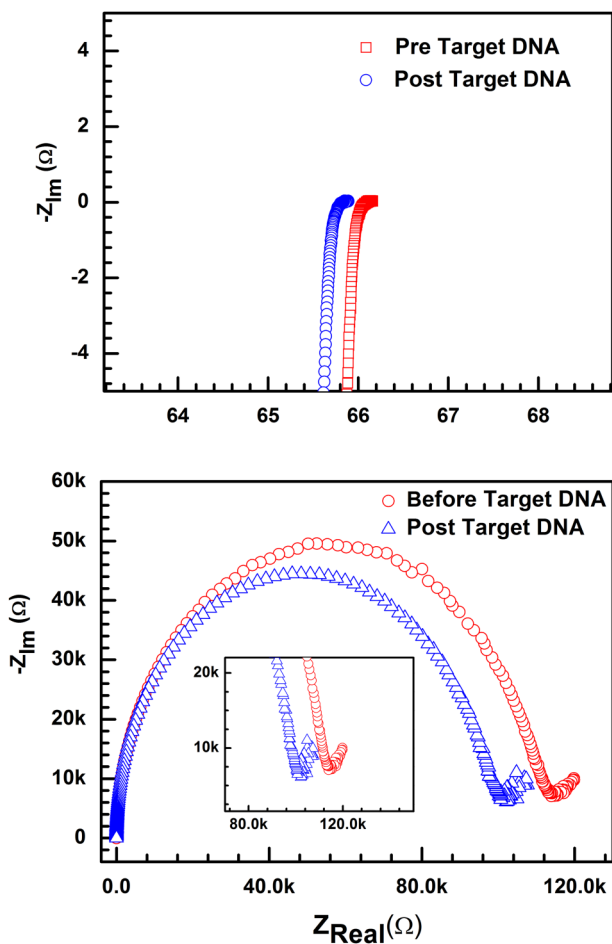


FIG. 5. EIS spectra from target-DNA attachment to SWCNT with probe-DNA are shown for ME and WE configurations for the target-DNA concentration of 1 fM.

MWCNT. For the DNA sensitivity experiments that follow, SWCNT is used as the packing material.

DNA hybridization experiments are carried out using a probe-DNA and a target-DNA that is perfectly matched. The DNA and the device protocol are described in detail in the Methods and Materials section. The initial EIS spectra in 1× PBS (SWCNT with probe-DNA only) and 1× PBS washing post target-DNA passage are acquired. The difference in the R_{ct} in the two EIS spectra is taken as the DNA hybridization signal. The change in the EIS spectra for two different electrode configurations, WE and ME, is shown in Fig. 5. As can be seen from Fig. 5, the difference between the impedance circuit indicates the binding of the target-DNA oligo to the probe-DNA. It is interesting to note that with the attachment of target-DNA, the R_{ct} is decreasing (Fig. 5). For SWCNT, carbon hybridizes into sp, sp² configurations with narrow gaps between their 2s and 2p electron shells. During the detection of DNA, as a π electron orbital is formed during the interaction of the double-stranded DNA with the SWCNT, specifically at the sp, sp² hybridization site. This π electron is often shared between the SWCNT and the double-stranded DNA.³² This manifests as an increased surface area of the transducer wherein the double-stranded

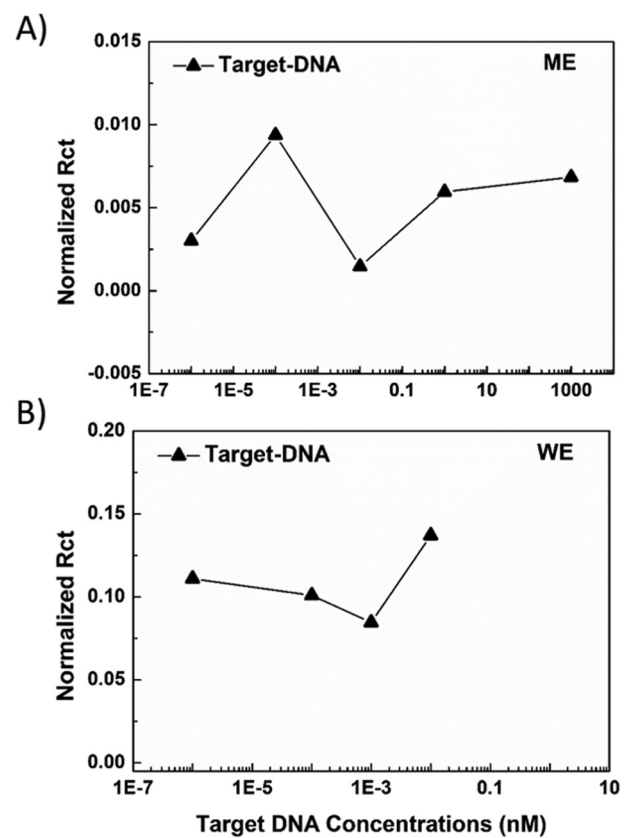


FIG. 6. The change in the normalized value of R_{ct} with changes in DNA concentration is plotted for the SWCNT electrode used in Fig. 5 for (a) ME and (b) WE configurations.

DNA acts as an extension of the SWCNT. This should lead to an increased ionic current, which translated to a decrease in R_{ct} .

However, to get a clear picture of the sensitivity of the different electrode configurations, the change in R_{ct} is normalized to the initial R_{ct} value of the device. This is also as the packing can change across devices. Even though the device loading is approximately the same, however, human error can lead to small variance during loading. Our earlier papers show that the EIS spectra of the device are dependent on the device structure.²⁵ Hence, a normalization would allow us to reduce/remove the variation due to packing. Figure 6 shows that post target-DNA hybridization, the ME shows a much smaller change in comparison to the WE (20 times). This is expected due to the current path in the two electrode configurations. Indeed as the ME is chiefly resistive, a small proportion of the current is carried by the ions. Hence, any changes in the overall current due to changes in the ionic current from the binding of the target-DNA are limited. The electric current through the SWCNT is unaffected by DNA binding, as the SWCNT is already very conductive. For the WE, the ionic current is the only way that the two sets of interdigitated electrodes can talk. Hence, changes in the SWCNT from the binding of the target-DNA are registered at significantly higher levels for WE.

It is important to note that the change in R_{ct} in Fig. 6 shows an increase with decreasing DNA, which is counterintuitive. It can be speculated here that there are two competing mechanisms for this decrease in R_{ct} . As detailed above, the sharing of the π electron cloud between the SWCNT and the double-stranded DNA manifests as a decrease in R_{ct} . However, as the amount of target-DNA coverage increases, it should lead to a progressive decrease in the amount of electrode surface area available to the transducer. This should lead to an increase in R_{ct} . Hence, the interplay between these two competing mechanisms makes the EIS change of the device is nonlinear with changing DNA concentration. Nevertheless, the sensitivity of the WE configuration in conjunction with the advantages of NP- μ IDE allows us to detect target-DNA rapidly, with high signal to noise at femtomolar levels.

CONCLUSION

To conclude, we demonstrated here that NP- μ IDE could be used in several different electrode configurations, WE, CE, and ME, to measure the binding of target-DNA to probe-DNA. The electrodes can be packed with different transducer materials. The packed NP- μ IDE electrode current has two current paths for ME. At low ionic strength and with conductive transducer materials like MWCNT, the current is chiefly electronic and can miss a contribution from the electrode-electrolyte interface. For conductive materials with charged moieties, such as C-SWCNT, the ionic current from the electrolyte-electrode interface is as strong as the electronic current at high ionic strength. The WE, on the other hand, will pick up any changes in the packed transducer material. However, due to the distance between the two pairs of NP- μ IDE in the WE configuration, scattering noise can dominate at low ionic strength. DNA sensitivity from both WE and ME configurations shows very high sensitivity (1 fM). However, the change in the R_{ct} from the binding of the target-DNA to the probe-DNA is 20 times larger for the WE configuration in contrast to the ME. Thus, the WE

configuration of the NP- μ IDE device can be used as a biosensor for the rapid detection of ctDNA in blood.

SUPPLEMENTARY MATERIAL

See the [supplementary material](#) for the EIS spectra from different target-DNA attachment to SWCNT with probe-DNA for the WE configuration. The target-DNA concentrations are (A) 10^{-2} nM, (B) 10^{-3} nM, (C) 10^{-4} nM, and (D) 10^{-6} nM.

ACKNOWLEDGMENTS

This manuscript is supported by Sagnik Basuray's National Science Foundation (NSF) under Grant No. 1751795, Career: 210 "ASSURED" electrochemical platform for multiplexed detection of Cancer Biomarker Panel using Shear Enhanced Nanoporous Capacitive Electrodes.

REFERENCES

- ¹H. Ilkhani and S. Farhad, *Anal. Biochem.* **557**, 151–155 (2018).
- ²R. Sharma, S. E. Deacon, D. Nowak, S. E. George, M. P. Szymonik, A. A. S. Tang, D. C. Tomlinson, A. G. Davies, M. J. McPherson, and C. Walti, *Biosens. Bioelectron.* **80**, 607–613 (2016).
- ³Y. Liu, M. Wang, E. M. Marcora, B. Zhang, and A. M. Goate, *Neurosci. Lett.* **711**, 134403 (2019).
- ⁴X. Li, M. Ye, W. Zhang, D. Tan, N. Jaffrezic-Renault, X. Yang, and Z. Guo, *Biosens. Bioelectron.* **126**, 596–607 (2019).
- ⁵L. Gorgannezhad, M. Umer, M. N. Islam, N. T. Nguyen, and M. J. A. Shiddiky, *Lab Chip* **18**(8), 1174–1196 (2018).
- ⁶L. Xi, T. H. Pham, E. C. Payabyab, R. M. Sherry, S. A. Rosenberg, and M. Raffeld, *Clin. Cancer Res.* **22**(22), 5480–5486 (2016).
- ⁷K. L. Spindler, N. Pallisgaard, R. F. Andersen, and A. Jakobsen, *Int. J. Cancer* **135**(9), 2215–2222 (2014).
- ⁸L. A. Diaz, Jr., R. T. Williams, J. Wu, I. Kinde, J. R. Hecht, J. Berlin, B. Allen, I. Bozic, J. G. Reiter, M. A. Nowak, K. W. Kinzler, K. S. Oliner, and B. Vogelstein, *Nature* **486**(7404), 537–540 (2012).
- ⁹A. Stahlberg, P. M. Krzyzanowski, M. Egyud, S. Filges, L. Stein, and T. E. Godfrey, *Nat. Protoc.* **12**(4), 664–682 (2017).
- ¹⁰A. Tadiyem, A. Closson, C. Li, S. Yi, T. Shen, and J. X. J. Zhang, *Crit. Rev. Clin. Lab. Sci.* **55**(3), 140–162 (2018).
- ¹¹J.-S. Do, Y.-H. Chang, and M.-L. Tsai, *Mater. Chem. Phys.* **219**, 1–12 (2018).
- ¹²E. O. Blair and D. K. Corrigan, *Biosens. Bioelectron.* **134**, 57–67 (2019).
- ¹³G. Luka, A. Ahmadi, H. Najjaran, E. Alcilja, M. DeRosa, K. Wolthers, A. Malki, H. Aziz, A. Althani, and M. Hoofar, *Sensors* **15**(12), 30011–30031 (2015).
- ¹⁴N. Bhalla, P. Jolly, N. Formisano, and P. Estrela, *Essays Biochem.* **60**(1), 1–8 (2016).
- ¹⁵S. Xu, J. Zhan, B. Man, S. Jiang, W. Yue, S. Gao, C. Guo, H. Liu, Z. Li, J. Wang, and Y. Zhou, *Nat. Commun.* **8**, 14902 (2017).
- ¹⁶Y. Huang, A. Hara, C. Terashima, A. Fujishima, and M. Takai, *Carbon* **152**, 354–362 (2019).
- ¹⁷G. Cabral-Miranda, A. R. Cardoso, L. C. S. Ferreira, M. G. F. Sales, and M. F. Bachmann, *Biosens. Bioelectron.* **113**, 101–107 (2018).
- ¹⁸J. E. Weber, S. Pillai, M. K. Ram, A. Kumar, and S. R. Singh, *Mater. Sci. Eng. C* **31**(5), 821–825 (2011).
- ¹⁹S. Ding, S. R. Das, B. J. Brownlee, K. Parate, T. M. Davis, L. R. Stromberg, E. K. L. Chan, J. Katz, B. D. Iverson, and J. C. Claussen, *Biosens. Bioelectron.* **117**, 68–74 (2018).
- ²⁰K. Awasthi, D. P. Singh, S. K. Singh, D. Dash, and O. N. Srivastava, *New Carbon Mater.* **24**(4), 301–306 (2009).

- ²¹K. Nagaraju, R. Reddy, and N. Reddy, *J. Appl. Biomater. Funct. Mater.* **13**(4), e301–e312 (2015).
- ²²A. Mirzapoor, A. P. F. Turner, A. Tiwari, and B. Ranjbar, *Mater. Sci. Eng. C* **104**, 109886 (2019).
- ²³H. Wang, L. Zhang, Y. Jiang, L. Chen, Z. Duan, X. Lv, and S. Zhu, *Sens. Actuators B* **261**, 441–450 (2018).
- ²⁴M. Varshney and Y. Li, *Biosens. Bioelectron.* **24**(10), 2951–2960 (2009).
- ²⁵Y.-H. C. Zhenglong Li, L. Feng, D. D. Felix, J. Neil, R. M. P. Antoni, M. Rahman, J. Yang, S. Azizighannad, S. Mitra, and S. Basuray, *J. Electrochem. Soc.* (unpublished).
- ²⁶S. Basuray, S. Senapati, A. Ajian, A. R. Mahon, and H. C. Chang, *ACS Nano* **3**(7), 1823–1830 (2009).
- ²⁷Z. El-Moussawi, A. Nourdine, H. Medlej, T. Hamieh, P. Chenevier, and L. Flandin, *Carbon* **153**, 337–346 (2019).
- ²⁸E. Katz and I. Willner, *Electroanalysis* **15**(11), 913–947 (2003).
- ²⁹G. Barbero and I. Lelidis, *Phys. Chem. Chem. Phys.* **19**(36), 24934–24944 (2017).
- ³⁰M. A. Atieh, O. Y. Bakather, B. Tawabini, B. Al-Tawbini, A. A. Bukhari, F. A. Abuilaiwi, and M. B. Fettouhi, *Bioinorg. Chem. Appl.* **2010**, 603978 (2010).
- ³¹Z. J. Tan and S. J. Chen, *Biophys. J.* **90**(4), 1175–1190 (2006).
- ³²G. Lu, P. Maragakis, and E. Kaxiras, *Nano Lett.* **5**(5), 897–900 (2005).